JOURNAL OF NATURAL PRODUCTS

pubs.acs.org/jnp

Article

Antiviral Activity of Cannabidiolic Acid and Its Methyl Ester against SARS-CoV-2

Martina Tamburello, Stefano Salamone, Lisa Anceschi, Paolo Governa, Virginia Brighenti, Alice Morellini, Giada Rossini, Fabrizio Manetti, Giorgio Gallinella, Federica Pollastro,* and Federica Pellati*

Cite This: *J. Nat. Prod.* 2023, 86, 1698−1707

Read Online

ACCESS | Metrics & More | Article Recommendations | Supporting Information

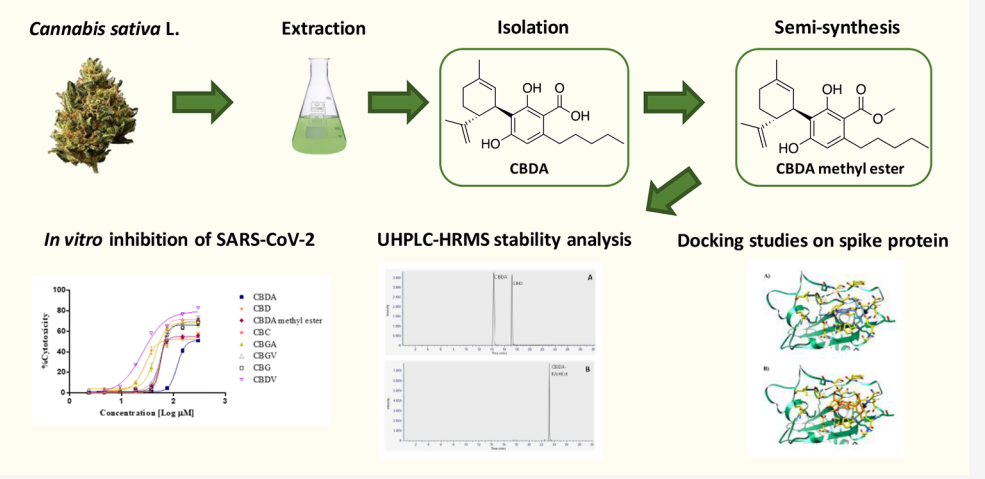

ABSTRACT: In the present study, the antiviral activity of cannabinoids isolated from *Cannabis sativa* L. was assessed *in vitro* against a panel of SARS-CoV-2 variants, indicating cannabidiolic acid (CBDA) was the most active. To overcome the instability issue of CBDA, its methyl ester was synthesized and tested for the first time for its antiviral activity. CBDA methyl ester showed a neutralizing effect on all the SARS-CoV-2 variants tested with greater activity than the parent compound. Its stability *in vitro* was confirmed by ultra-high-performance liquid chromatography (UHPLC) analysis coupled with high-resolution mass spectrometry (HRMS). In addition, the capacity of both CBDA and its derivative to interact with the virus spike protein was assessed *in silico*. These results showed that CBDA methyl ester can be considered as a lead compound to be further developed as a new effective drug against COVID-19 infection.

Severe acute respiratory syndrome coronavirus 2 (SARS-CoV-2) is the etiological cause of Coronavirus disease 2019 (COVID-19), which led to a global pandemic.[1]

SARS-CoV-2 is thought to infect cells after binding with high affinity to a host cell receptor through the interaction of its spike protein with the angiotensin-converting enzyme 2 (ACE2) receptors,[2] which are widely expressed in nasal and oral mucosa as well as in the lungs and gastrointestinal tract. The spike protein binds primarily to ACE2 on target cells, and it is then processed by membrane proteases, leading to viral internalization via fusion with the plasma membrane.[2,3]

COVID-19 pathogenesis is characterized by two main aspects; in the early stage of the infection, it is primarily driven by the replication cycle of SARS-CoV-2, which is mainly modulated by viral proteins, while, in the late stage of the infection, it is associated with an abnormal inflammatory and immune response that results in tissue damage.[4] Thus, both the proteins of the virus and the host factors are promising potential targets for efficient antiviral therapies.[4,5]

Recent scientific research has been focused on both the repurposing of existing drugs and the discovery of new compounds for the prevention and treatment of COVID-19.[6] In addition to vaccines, small molecules, including natural compounds, may play a role in the management of this disease.[6] Natural products and their metabolites isolated from

Received: February 8, 2023
Published: July 4, 2023

various plants have been described to possess striking inhibitory action against different SARS-CoV-2 proteins.[7]

Cannabinoids from *Cannabis sativa* L. have been studied for many therapeutic properties, including for anti-inflammatory, antimicrobial, and antiproliferative activity.[8,9] Among these compounds, those that are most worth studying are the non-psychoactive ones, which have no collateral psychotropic effects, due to interaction with CB1 receptors, and are more suitable for long-term use. Published preclinical studies show cannabinoids as promising antiviral compounds, even if limited evidence demonstrates their possible role as therapeutics against viral diseases.[10]

Recent studies have highlighted that cannabidiol (CBD) exerts beneficial effects in viral infections, such as in COVID-19, in which the inflammatory response is pathogenic,[11] where SARS-CoV-2 virus triggers a cytokine storm.[10,12] Indeed, the severity of COVID-19 is generally associated with a cytokine storm, primarily caused by the pro-inflammatory cytokines IL-6, IL-8, and TNF-α, the overproduction of which leads to impaired oxygen diffusion, pulmonary fibrosis, and multiorgan failure.[13] *In vivo* studies have demonstrated the inhibitory effect of cannabinoids on the course of cytokine storms, improvement of lung tissue function, and reduction in inflammation,[13,14] which may be helpful in the treatment of COVID-19.

Recently, *in silico* studies have rationalized the capacity for cannabinoids to inhibit the viral spike−ACE2 complex[15] and their additional interaction with viral enzymes, i.e., the SARS-CoV-2 main protease (Mpro) and the papain-like protease (PLpro), that serve as principal therapeutic targets to prevent SARS-CoV-2 replication.[16] In addition, the role of CBD in blocking viral replication by inhibiting SARS-CoV-2 Mpro has been demonstrated both *in silico* and *in vitro*.[17] Moreover, an *in vitro* study has shown the reduction of the ACE2 receptor expression in epithelial cells of lung tissue after administration of CBD.[18] Nguyen et al. demonstrated that CBD inhibits infection of SARS-CoV-2 in both cells and mice.[19] In particular, CBD and its metabolite 7-OH-CBD, but not Δ^9-tetrahydrocannabinol (Δ^9-THC) or other cannabinoids tested, potently block SARS-CoV-2 replication in lung epithelial cells through the viral gene expression inhibition and reversing many effects of the virus on host gene transcription.[19] This latter action has been supported by Wang et al. (2020), who have identified high-CBD *C. sativa* extracts that are able to decrease ACE2 protein levels in artificial 3D human models of the oral, airway, and intestinal tissues.[20] Furthermore, some *C. sativa* extracts down-regulated serine protease TMPRSS2, another critical protein required for SARS-CoV-2 entry into host cells.[20]

Recently, cannabigerolic acid (CBGA) and cannabidiolic acid (CBDA) have been found to prevent the entry of SARS-CoV-2 into human epithelial cells with similar effects against both alpha and beta variants of SARS-CoV-2.[21] The authors have demonstrated that these compounds prevented the infection of human epithelial cells by a pseudovirus that expressed the SARS-CoV-2 spike protein and prevent the entry of live SARS-CoV-2 into cells.[21]

To provide further insight into the potential role of naturally occurring cannabinoids as antiviral agents against SARS-CoV-2, in the present study, the antiviral activity of cannabinoids isolated from *C. sativa* was assessed *in vitro* against a panel of virus variants. To overcome the issue of the very limited stability of CBDA, which, as with other cannabinoic acids, can easily undergo a spontaneous decarboxylation leading to its neutral counterpart CBD, the semisynthesis of its methyl ester (also known as HU-580) was carried out and the activity of the derivative was assessed for the first time. Indeed, the limited stability of CBDA negatively affects its bioactivity profile, thus enhancing the chance of compound attrition in the early phase of the drug discovery process.[22] Interestingly, CBDA methyl ester showed a good neutralizing effect on all the tested SARS-CoV-2 variants, and its stability after the *in vitro* administration was confirmed using ultra-high-performance liquid chromatography (UHPLC) coupled with high-resolution mass spectrometry (HRMS) analysis, performed on cell lysates after the treatments. Finally, the capacity of both CBDA and its methyl ester to interact with the virus spike protein was assessed *in silico*.

RESULTS AND DISCUSSION

In the present study, a group of cannabinoids with different structures were isolated from non-psychoactive *C. sativa*, and their antiviral activity against SARS-CoV-2 was assessed. During the screening and in subsequent assays, two compounds exhibited a broad inhibitory effect against SARS-CoV-2 PV10734 Italian strain and a panel of SARS-CoV-2 variants, including Delta (lineage B.1.167.2) and variants of concern (VOCs) Omicron BA.1, Omicron BA.2, Omicron BA.3, Omicron BA.4, and Omicron BA.5.

Structural Characterization of Natural and Synthetic Cannabinoids. The isolated cannabinoids, including CBGA (**1**, Figure S1) and CBDA (**2**, Figure S2), were obtained in their genuine acidic form from the plant material, together with their neutral counterparts cannabigerol (CBG, **5**, Figure S5) and CBD (**3**, Figure S3) after the decarboxylation process. In addition, the purification process allowed us to isolate cannabichromene (CBC, **4**, Figure S4) and the propyl derivatives cannabidivarin (CBDV, **6**, Figure S6) and cannabigerovarin (CBGV, **7**, Figure S7). CBDA was semisynthesized as the corresponding methyl ester (**8**, Figure S8) to preserve the carboxylic moiety, which undergoes a natural nonenzymatic decarboxylation process, strongly affecting its stability.[23]

Evaluation of SARS-CoV-2 CPE Inhibition. A group of cannabinoids was chosen to evaluate their antiviral activity against the Italian strain SARS-CoV-2 PV10734 (D614G, lineage B.1.1) and a panel of local isolates collected in the period January−May 2022, including variants Delta (B.1.167.2) and VOCs Omicron BA.1, BA.2, BA.3, BA.4, and BA.5 by using an *in vitro* assay model.

Cytotoxicity evaluation was carried out in the concentration range between 2.3 and 300.0 μM (Figure S9). The cytotoxic activity of cannabinoids toward Vero E6 cells, represented by CC_{50} (50% cytotoxic concentration), is shown in Table 1.

Compounds with CC_{50} values greater than or equal to 50 μM were used in the cytopathic effect (CPE) neutralization assay to determine whether they can inhibit virus-induced cytopathic effects in cells. The cytopathic effect is the phenotypic consequence of host cell death related to viral replication, and, therefore, it is a simple and rapid assay for the screening of compounds with potential antiviral activity against SARS-CoV-2.[23−27] Microscopic observation showed CPE was blocked for SARS-CoV-2 PV10734, Delta, and VOCs Omicron BA.1, BA.2, BA.3, BA.4, and BA.5 preincubated with CBDA and CBDA methyl ester at the concentrations of 75.0 and 37.5 μM, respectively (Figure S10). In addition, the two compounds showed a similar inhibitory activity across the

https://doi.org/10.1021/acs.jnatprod.3c00111
J. Nat. Prod. 2023, 86, 1698−1707

Table 1. CC_{50} Values of Cannabinoids and Derivatives, Determined Using the Nonlinear Regression Dose−Response Curve

compound	CC_{50} (μM) ± SD
CBDA	118.6 ± 2.2
CBD	28.9 ± 1.5
CBDA methyl ester	52.4 ± 2.5
CBC	59.3 ± 0.3
CBGA	43.9 ± 3.4
CBGV	58.1 ± 0.6
CBG	58.0 ± 3.4
CBDV	26.0 ± 0.2

SARS-CoV-2 variants and the Italian strain SARS-CoV-2 PV10734 at the concentrations tested. The other cannabinoids showed no relevant inhibition of the cytopathic effect under the conditions tested (data not shown), and, therefore, they were not used in subsequent assays.

Viral Titers Were Significantly Inhibited by CBDA and CBDA Methyl Ester in a Tissue Culture Infectious Dose ($TCID_{50}$/mL) Assay. The extent of viral replication was measured in the CPE assay medium by the calculation of tissue culture infectious dose per mL ($TCID_{50}$/mL), according to Reed and Muench method,[28] which is a traditional method to quantify the infectious titer by end point titration, defined as the burden of viral infectious particles per unit volume capable of producing a cytopathic effect in half of the infected cell culture.[28−30]

CBDA and its methyl ester significantly reduced viral titers of progeny viruses collected from the supernatants of all SARS-CoV-2 strains tested, including VOCs (Figure 1A−G), with greater than 90% inhibition at 75.0 and 37.5 μM, respectively (Figure 1H−N).

These results confirmed the suppressive effects of the two cannabinoids. As shown in Table 2, CBDA and its methyl ester significantly reduced viral titers of progeny viruses collected from the supernatants of all SARS-CoV-2 strains tested, including Delta and Omicron BA.1, BA.2, BA.3, BA.4, and BA.5, indicating no substantial loss of activity against VOCs.

CBDA and Its Methyl Ester Reduce SARS-CoV-2 Viral Load by qRT-PCR. Quantitative RT-PCR (qRT-PCR) was performed targeting the E gene, RdRP/S gene, and N gene of SARS-CoV-2. The viral load (cp/μL) of each SARS-CoV-2 strain tested was calculated by the absolute quantification of the N gene by interpolation in a parallel calibration curve. These results confirmed that at 72 hpi both CBDA and its methyl ester, preincubated with the viral strains, reduced the replication of SARS-CoV-2 PV10734 and variants Delta and Omicron BA.1, BA.2, BA.3, BA.4, and BA.5 with increased activity at the concentrations of 75.0 and 37.5 μM, respectively (Figure 2).

Both CBDA and its methyl ester demonstrated comparable activity to the two quantification methods. The differences observed are because the $TCID_{50}$/mL method measures the ability of the virus present in the specimen to infect cells and to produce a visible cytopathic effect, while qRT-PCR could lead to an overestimation of the titer by detecting the total amount of RNA molecules, including both genomic RNA and subgenomic mRNAs.[31]

The results obtained from the inhibition assays are consistent with previous studies on the ability of cannabinoids to prevent virus entry into epithelial cells.[21] Therefore, the neutralization data obtained from the preincubation of the virus with the compounds suggest that CBDA and its methyl ester can block SARS-CoV-2 before cell entry; even a possible involvement in the steps following viral entry cannot be excluded and should be further investigated.

UHPLC-HRMS Analysis of Cell Lysates and Culture Media. Cell lysates from Vero E6 cells and culture media from the different treatment groups (CBDA, CBDA methyl ester, and control) were analyzed by UHPLC-HRMS with the purpose of determining if either the active compounds undergo metabolic transformations or are still active in their original form after the administration. The attention was focused on CBDA, its decarboxylation product CBD, and CBDA methyl ester using HRMS parameters carefully optimized with pure compounds. In addition, degradation compounds structurally related to CBD, such as CBD-hydroxyquinone (also known as HU-331), which can be generated under oxidative conditions, were monitored. In an attempt to investigate the presence of these compounds in cell lysates and culture media, targeted metabolomic analysis was carried out.

Figure 3 shows representative UHPLC-HRMS chromatograms of both cell lysates and culture media obtained from Vero E6 cells 72 h after treatment with CBDA and its methyl ester. From the experimental data, it is possible to conclude that, when cells are treated with CBDA, there is a consistent decarboxylation of this compound into its neutral counterpart CBD. This can be seen in cell lysates (Figure 3A), where the ratio between CBDA and CBD is almost 1:1, based on peak area. On the contrary, only the semisynthetic derivative CBDA methyl ester was identified in cell lysates after the treatment as well as in the culture media (Figure 3B and D). The rapid degradation of CBDA into CBD may be the reason that CBDA was active in neutralizing SARS-CoV-2 at higher concentrations than its methyl ester.

Based on both the bioactivity and stability data, CBDA methyl ester can be considered as a new lead compound for the development of an innovative drug against SARS-CoV-2 viral infection.

***In Silico* Assessment of the Interaction with SARS-CoV-2 Spike Protein.** Van Breemen and co-workers have recently suggested a possible binding mode for CBDA into the orthosteric binding site of SARS-CoV-2 spike protein.[21] To evaluate the possible binding of CBDA methyl ester and SARS-CoV-2 spike protein, a molecular docking simulation was performed using the same crystal structure (PDBID: 6lzg) and the same docking software (AutoDock Vina) previously described by Van Breemen and colleagues.[21]

A blind docking procedure was applied to confirm that CBDA could preferentially bind the orthosteric binding site, and the results obtained are comparable to those previously described in the literature,[21] with a very similar binding pose (Figure 4A).

Among the possible binding modes predicted for CBDA methyl ester through docking, one was very similar to that of CBDA (Figure 4B). Indeed, one of the major anchor points is represented by the same hydrogen bond between the hydroxy group in position 4 and the backbone NH of Gly496. Moreover, the isopropenylmethylcyclohexenyl moiety is positioned in the proximity of Gln498, Asn501, Gly502, and Tyr505, which gave hydrophobic interactions with both ligands. Other conserved interactions include van der Waals contacts with Tyr453, Tyr449, Tyr495, Phe497, and Gln498. The presence of the methyl ester moiety in the CBDA

https://doi.org/10.1021/acs.jnatprod.3c00111
J. Nat. Prod. 2023, 86, 1698−1707

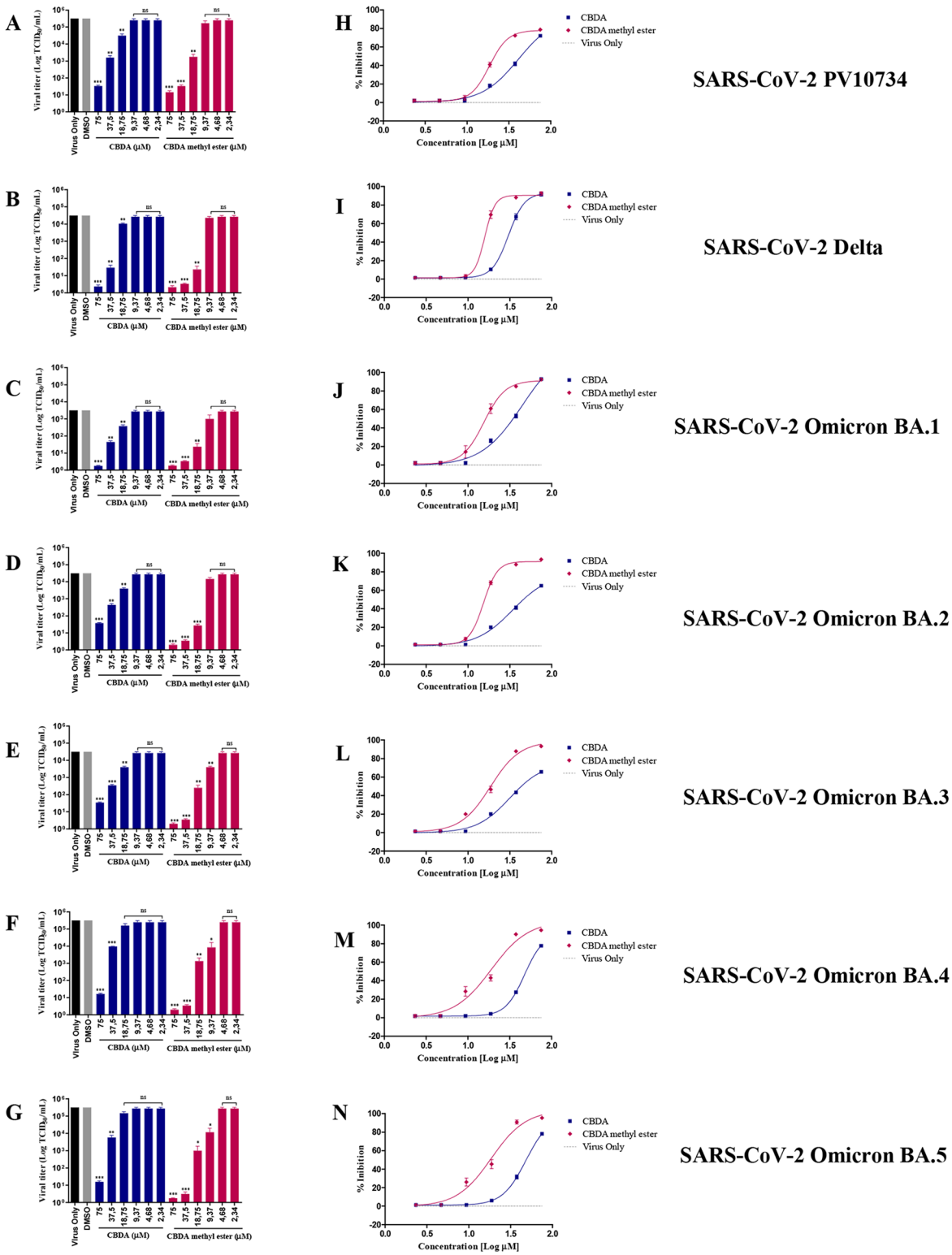

Figure 1. Effect of CBDA and its methyl ester on viral titers of SARS-CoV-2 Italian strains (PV10734) and VOCs by the tissue culture infectious dose ($TCID_{50}$/mL) assay. A, B, C, D, E, F, and G: The virus titers (log $TCID_{50}$/mL) in the supernatants of Vero E6 cells infected with SARS-CoV-2 PV10734, Delta, Omicron BA.1, Omicron BA.2, Omicron BA.3, Omicron BA.4, and Omicron BA.5 and treated with scalar doses of CBDA and CBDA methyl ester were determined by tissue culture infectious dose per mL ($TCID_{50}$/mL) assay, calculated by using the Reed and Muench method. The data are represented as the mean ± SD from three independent experiments (***$p \leq 0.001$, **$p \leq 0.01$, *$p \leq 0.05$, ns $p \geq 0.05$). H, I, J, K, L, M, N: % inhibition of CBDA and its methyl ester for each SARS-CoV-2 strain tested. The *y*-axis indicates the inhibition of virus titer (percent) relative to that of the untreated control group (Virus Only). The *x*-axis indicates the concentration (log) of inhibitors.

https://doi.org/10.1021/acs.jnatprod.3c00111
J. Nat. Prod. 2023, 86, 1698−1707

Table 2. IC_{50} Values of CBDA and Its Methyl Ester, Specific for Each SARS-CoV-2 Strain Tested, Calculated from Virus Titers ($TCID_{50}$/mL) Using a Nonlinear Regression Curve

compound	virus variant	IC_{50} value (μM) ± SD
CBDA	SARS-CoV-2 PV10734	42.7 ± 7.4
	Delta	30.7 ± 2.7
	Omicron BA.1	45.4 ± 7.5
	Omicron BA.2	35.1 ± 7.0
	Omicron BA.3	31.7 ± 3.3
	Omicron BA.4	47.7 ± 11.2
	Omicron BA.5	47.5 ± 4.2
CBDA methyl ester	SARS-CoV-2 PV10734	18.4 ± 1.3
	Delta	15.9 ± 0.9
	Omicron BA.1	15.5 ± 2.6
	Omicron BA.2	16.6 ± 0.8
	Omicron BA.3	18.6 ± 2.0
	Omicron BA.4	19.0 ± 1.1
	Omicron BA.5	18.6 ± 1.3

derivative prevents the formation of the hydrogen bond between the carboxyl group in CBDA and Arg403, due to steric hindrance. This could be the cause of the reduction in the binding energy from −5.6 kcal/mol to −4.5 kcal/mol for CBDA and its methyl ester, respectively.

The results of the docking simulations, which predicted more profitable interactions of CBDA in comparison to CBDA methyl ester (in terms of binding energy and hydrogen bonding with Arg403), appeared in disagreement with experimental results that showed a better activity for the methyl ester. However, this discrepancy could be accounted for by the higher stability of the CBDA methyl ester compared to CBDA. Indeed, a fast decarboxylation of CBDA occurred in the cell lysate, thus leading to the neutral CBD and preventing the predicted hydrogen bond between Arg403 and the carboxylic acid moiety of CBDA, which served as one of the anchor points for the binding of CBDA itself.

Overall, docking simulations support the hypothesis that CBDA methyl ester could bind the orthosteric binding site of the SARS-CoV-2 spike protein, with binding similar to that of CBDA.

EXPERIMENTAL SECTION

General Experimental Procedures. Silica gel 60 (0.063−0.200 mm), reversed-phase (RP) C_{18} silica gel (25 μm), and Celite 545 particle size 0.02−0.1 mm, used for low-pressure liquid chromatography (LPC) and vacuum chromatography, were purchased from Macherey-Nagel (Düren, Germany). Purifications were monitored by TLC on Merck 60 F254 (0.25 mm) plates and visualized by staining with 5% H_2SO_4 in EtOH and heating.

Standard solutions of CBDA and CBD (1 mg/mL in acetonitrile) were purchased from Restek (Milan, Italy). Analytical grade petroleum ether (PE), ethyl acetate (EtOAc), dichloromethane (DCM), acetone, acetonitrile (ACN), ethanol (EtOH), methanol (MeOH), sodium hydroxide (NaOH), sulfuric acid (H_2SO_4), formic acid (HCOOH), and anhydrous sodium sulfate (Na_2SO_4), were from Sigma-Aldrich (Milan, Italy). Water (H_2O) was purified using a Milli-Q Plus185 system from Milli-Q (Milford, MA, USA).

A flash chromatography Isolera One automated system with UV/DAD detection (Uppsala, Sweden) was used. ^{1}H NMR 400 MHz spectra were measured on Bruker 400 spectrometers (Bruker, Billerica, MA, USA). Chemical shifts were referenced to the residual solvent signal ($CDCl_3$: δ_H = 7.26).

Plant Material. Non-psychoactive *Cannabis sativa* L. plant material, belonging to a CBDV-rich chemotype, was purchased from Canvasalus Srl (Monselice, Italy). A voucher specimen (Cs-G309/12/2022) of the vegetal material is stored in Novara Laboratories.

Extraction and Isolation. Nonwoody *C. sativa* aerial parts (228 g), including inflorescences and leaves, were extracted with acetone (2 × 10 L) in a vertical percolator at room temperature, affording 15.6 g (6.9%) of a dark green syrup. This was later dissolved at 45 °C in 150 mL of MeOH (with a raw extract/MeOH ratio corresponding to 1:10 w/v) and left at 8 °C to condense fatty acids and waxes. After 12 h, the solution was vacuum-filtered with cold MeOH in a sintered funnel protected by a bed of stratified Celite, obtaining 11.7 g of residual fraction after evaporation of solvent with a rotary evaporator. This latter part was subsequently purified by solid-phase extraction on C_{18} silica gel to remove pigments, unsaturated fatty acids, and poly isoprenoids. For this purpose, the fraction was dissolved in the minimal MeOH amount at 45 °C and charged on 110 g of C_{18} (with a raw extract/stationary phase ratio of 1:10 w/w), packed with MeOH in a sintered funnel (9 × 15 cm) with a side arm for vacuum. Elution with MeOH (100 mL) gave 10 g of the purified fraction.

Fractionation of Cannabinoic Acids. The defatty extract was dissolved in 100 mL of PE and 10 mL of acetone in a separating funnel and partitioned twice with 250 mL of NaOH 2% in H_2O. The basic solution containing the sodium salt of cannabinoic acids was then acidified to pH 3 with H_2SO_4 until the formation of a milky mixture due to the insolubility of cannabinoic acids under acidic conditions. This latter acidified fraction was then partitioned with DCM (2 × 110 mL), anhydrified with Na_2SO_4, and completely evaporated, affording 7.6 g of raw cannabinoic acid fraction.

Purification of Cannabinoic Acids. A portion of 2.5 g of the raw cannabinoic acid fraction was purified by LPC on silica gel (150 g, PE−EtOAc gradient from 70:30 to 20:80 v/v) to afford three fractions (I, II, and III). Fraction I, consisting of 1.3 g of a mixture of CBGA (**1**)[32] and CBDA (**2**),[32] was further purified by flash chromatography with Isolera One on RP_{18} silica gel (12 g, solvent A: MeOH 0.03% formic acid, solvent B: H_2O 0.03% formic acid gradient from 50:50 to 95:5) to afford 317 mg of CBDA (**2**) and 380 mg of CBGA (**1**), respectively.[32]

Decarboxylation and Cannabinoid Purification. A portion of 5 g of the raw cannabinoic acid fraction was heated at 130 °C under stirring for 45 °C in a paraffin bath to achieve the decarboxylation of the cannabinoic acids. The reaction was followed by TLC on silica with a mobile phase composed of petroleum ether and EtOAc (80:20, v/v). This latter decarboxylated fraction was fractionated by LPC on silica gel (250 g, PE−EtOAc gradient from 90:10 to 20:80 v/v) to afford three fractions (I, II, and III). Fraction I (1.3 g) was further purified with LPC on silica gel (75 g, PE−EtOAc gradient from 90:10 to 80:20 v/v) to afford, after diethyl ether crystallization, 643 mg of CBD (**3**)[33] as a white powder, 96 mg of CBC (**4**)[34] as brownish powder, and 772 mg of CBG (**5**)[33] as a white powder. Fraction II (2.8 g) was fractionated with LPC on silica gel (130 g, PE−EtOAc gradient from 80:20 to 70:30 v/v) to afford, after diethyl ether crystallization, 1.296 g of CBDV (**6**)[35] and 1.248 g of CBGV (**7**)[35] both as a white powder. All of the isolated compounds were identified according to ^{1}H NMR previously described in the literature. NMR data of the isolated compounds are shown in Figures S1−S8 of the Supporting Information.

Esterification of CBDA. CBDA methyl ester (**8**) has been previously synthesized by Mechoulam and Gaony in 1965,[32] starting from a crude *C. sativa* extract and treatment with diazomethane. To avoid the formation of undesired products, such as CBDA methyl ether and methyl ester, a solution of CBDA (**2**, 100 mg, 0.279 mmol) in MeOH (5 mL) was treated with a catalytic quantity of *p*-toluenesulfonic acid (*p*-TSA) and *N,N′*-dicyclohexylcarbodiimide (DCC, 115.13 mg, 2 equiv/mmol). The reaction was followed by TLC on silica using a mobile phase composed of PE−EtOAc (80:20, v/v) by monitoring the disappearance of **2**. After stirring for 1 h at room temperature, the solvent was evaporated under reduced pressure, and the residue dissolved in toluene and placed at 8 °C for 3 h to remove by filtration the dicyclohexylurea (DCU). After solvent evaporation at the rotary evaporator, the final residue was

https://doi.org/10.1021/acs.jnatprod.3c00111
J. Nat. Prod. 2023, 86, 1698−1707

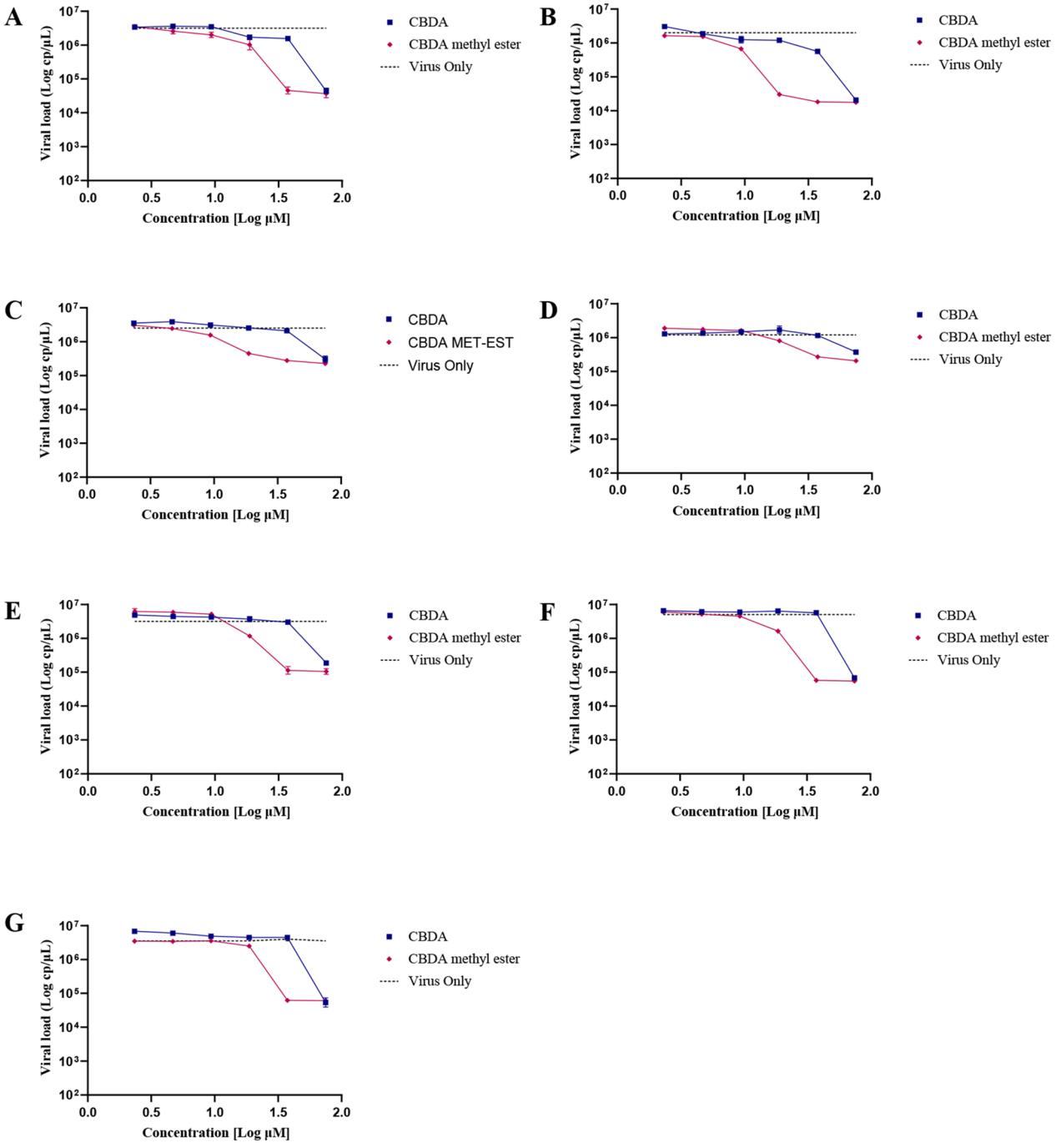

Figure 2. Effect of CBDA and its methyl ester on viral load (cp/μL) of SARS-CoV-2 by qRT-PCR. The viral load (log cp/μL) quantified by qRT-PCR in the supernatants of Vero E6 cells infected with SARS-CoV-2 PV10734 (A), Delta (B), Omicron BA.1 (C), Omicron BA.2 (D), Omicron BA.3 (E), Omicron BA.4 (F), and Omicron BA.5 (G) and treated with scalar doses of CBDA and CBDA methyl ester (log μM). The data are shown as the mean ± SD from three independent experiments.

purified with HPLC on silica (PE−EtOAc gradient from 95:5 to 90:10 v/v) to afford 90.9 mg of CBDA methyl ester[32] (**8**, 0.244 mmol, 87.5% based on conversion of **2**) as a yellow oil.

*CBDA methyl ester (**8**):* $C_{23}H_{32}O_4$, MW 372.51; ^{1}H NMR ($CDCl_3$, 400 MHz) δ_H 4.11 (1H, s, H-1); 5.56 (1H, s, H-2); 2.20 (1H, m), 2.10 (1H, m, H-4); 1.86 (2H, m, H-5); 2.40 (1H, m, H-6); 1.80 (3H, *s*, H-7); 4.54 (*trans*, 1H, *m*), 4.41 (*cis*, 1H, m, H-9); 1.72 (3H, s, H-10); 6.54 (1H, s), 6.54 (1H, s, 5′-OH); 2.86 (1H, m), 2.78 (1H, m, H-1″); 1.57 (2H, m, H-2″); 1.33 (4H, m, H-3″); 1.33 (4H, m, H-4″); 0.89 (3H, t, H-5″); 6.24 (1H, s, 1″-OH); 3.91 (3H, s, OMe); HRMS $[M - H]^-$ m/z 371.2232 (calcd for $C_{23}H_{31}O_4$ 371.2222); UV spectrum λ_{max} = 225 nm; FR-IR spectra ν_{max} 3416, 2927, 1647, 1621, 1577, 1435 cm^{-1}.

Cells and Culture Conditions. Vero E6 cells (ATCC CRL-1586) were cultured in Dulbecco's modified Eagle's medium (DMEM, EuroClone, Milan, Italy), supplemented with 2 mM L-glutamine (EuroClone, Milan, Italy), 10% fetal bovine serum (Gibco, Thermo Fisher, Monza, Italy), and 1% penicillin/streptomycin solution (EuroClone, Milan, Italy) and passaged twice per week at 1:4 dilutions using trypsin−EDTA (EuroClone, Milan, Italy). Briefly, cell culture media were aspirated, and cells were washed with phosphate-buffered saline (PBS). Then 3 mL of trypsin was added for

https://doi.org/10.1021/acs.jnatprod.3c00111
J. Nat. Prod. 2023, 86, 1698−1707

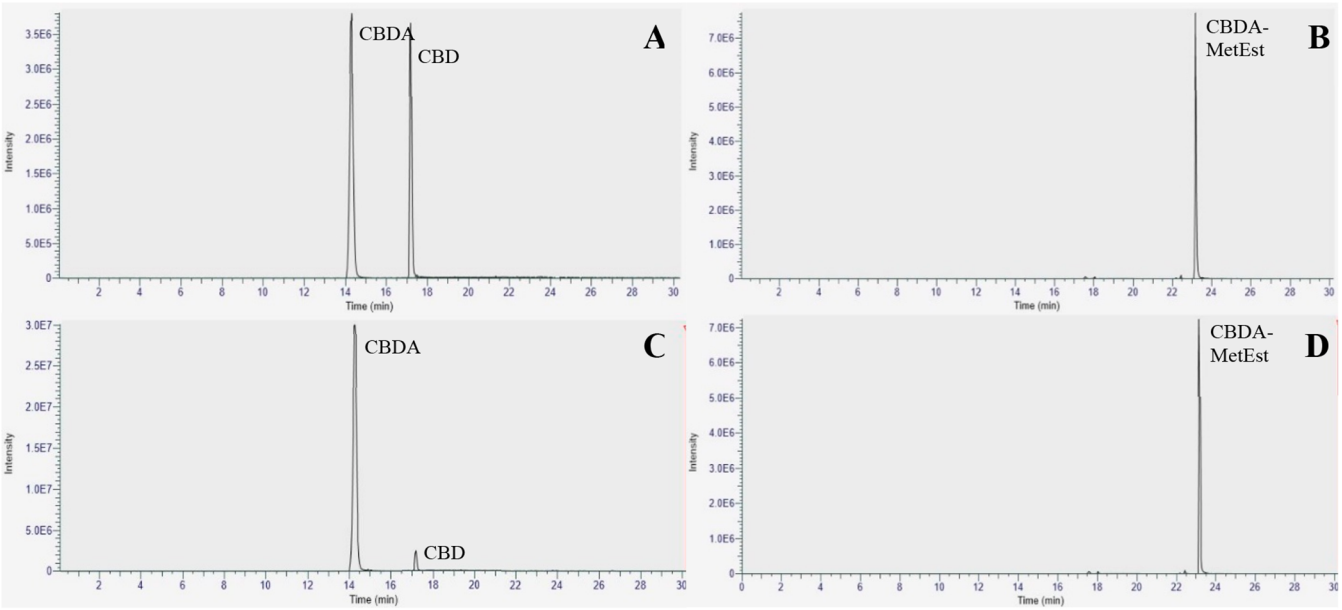

Figure 3. Representative UHPLC-HRMS (full-scan) chromatograms of Vero E6 cell lysates after 72 h of treatment with CBDA and its methyl ester. The plots are related to cell lysates (A, B) obtained from Vero E6 cells treated with CBDA at 75.0 μM (A) and CBDA methyl ester at 37.5 μM (B); culture media obtained from cells treated with CBDA (C) and CBDA methyl ester (D). Analyses were performed in duplicate for each experimental condition.

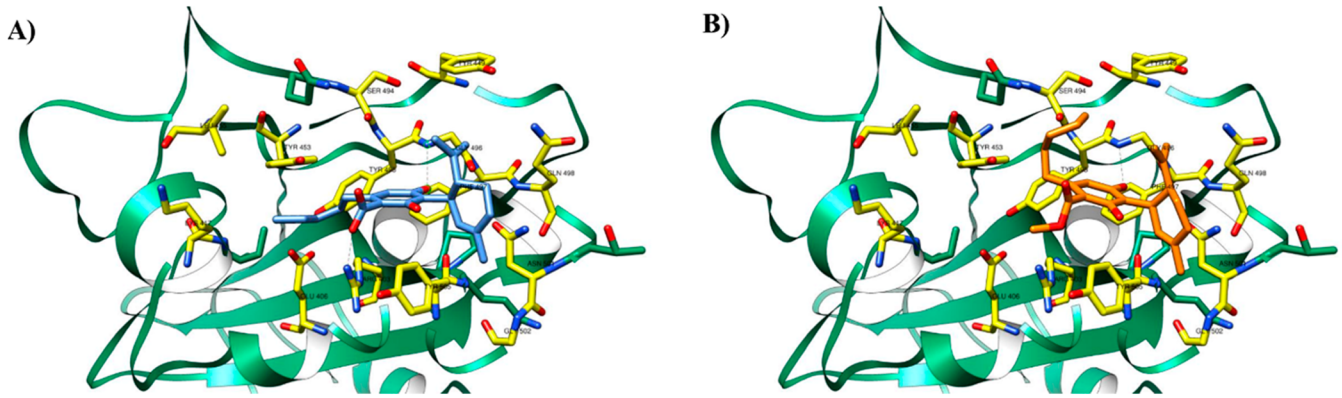

Figure 4. Docking pose of (A) CBDA (pale blue sticks) and (B) CBDA methyl ester (orange sticks) in the orthosteric binding site of the SARS-CoV-2 spike protein. The binding site residues are shown as yellow sticks. Dashed green lines correspond to hydrogen bonds.

1−2 min at 37 °C, and 9 mL of DMEM was added to create a single-cell suspension. Cells were centrifuged at 1500 rpm for 3 min and then resuspended in fresh medium for seeding into flasks.

Viral Strains and Titration. The clinical isolate of SARS-CoV-2 Italian strain PV10734 (D614G, lineage B.1.1) was obtained from Fondazione IRCCS Policlinico San Matteo (Pavia, Italy). The other strains including the Delta variant (lineage B.1.167.2) and VOCs including Omicron BA.1 and Omicron BA.2 (GenBank: EPI_ISL_15088435), Omicron BA.3 and Omicron BA.4 (GenBank: EPI_ISL_12529661), and Omicron BA.5 (GenBank: EPI_ISL_15088465) were isolated from nasal swabs of adult patients diagnosed with COVID-19 at S. Orsola-Malpighi Hospital (Bologna, Italy) in January−May 2022, in the course of institutional diagnostic activity. The identity of SARS-CoV-2 strains was established by sequencing[36] and confirmed with a database of sequence data of the viruses. All the strains were propagated in Vero E6 cells as described before[29,37] and stored at −80 °C. The viral titer was determined by the $TCID_{50}$/mL method.[28] The infection experiments were performed in a biosafety level-3 (BLS-3) laboratory.

Preparation of Test Compounds. The tested cannabinoids were dissolved in dimethyl sulfoxide (DMSO) and diluted with DMSO to the desired concentration for *in vitro* assays.

Cytotoxicity Assay. The cytotoxic effect of all cannabinoids was evaluated using the Vero E6 cell line in a biosafety level-2 (BLS-2) laboratory. Vero E6 were seeded in a 96-well tissue culture microplate (2×10^4 cells/well) and incubated in a 5% CO_2 incubator at 37 °C overnight. Each test compound was diluted with DMSO and added to the cells at final concentrations of 2.3, 4.7, 9.4, 18.8, 37.5, 75.0, 150.0, and 300.0 μM. DMSO concentration was normalized to 0.5% v/v to minimize the cytotoxic effect. After 72 h of incubation, cytotoxicity was determined using the cytotoxicity LDH assay kit−WST (Dojindo Molecular Technologies Inc.), following the manufacturer'sprotocol, and the absorbance was measured at 490 nm. The percentage of cell cytotoxicity was calculated by comparing the absorbance value of the test compound to DMSO as a control. Data were expressed as 50% cytotoxic concentration (CC_{50}), which was determined by the nonlinear regression dose−response curve using GraphPad Prism version 8.4.2. Further assays were focused on cannabinoids with CC_{50} values above 50 μM.

https://doi.org/10.1021/acs.jnatprod.3c00111
J. Nat. Prod. 2023, 86, 1698−1707

***In Vitro* SARS-Cov-2 Neutralization CPE Assay.** Neutralization of SARS-CoV-2 strains was performed using a cytotoxic effect assay. Briefly, Vero E6 cells were seeded in triplicate in a 96-well tissue culture microplate (2×10^4 cells/well) and incubated in a 5% CO_2 incubator at 37 °C overnight. Serial dilutions of selected cannabinoids from 75.0 to 2.3 μM were prepared by using DMEM supplemented with 2% fetal bovine serum (FBS) in a 96-well tissue culture plate, and an equal volume of the SARS-CoV-2 PV10734 strain or the variants (Delta, Omicron BA.1, BA.2, BA.3, BA.4, and BA.5) containing 100 $TCID_{50}$ per well was added and then incubated at 37 °C for 1 h. DMSO was used as the vehicle control. After incubation, the cannabinoids−virus mixture was transferred into a 96-well plate containing subconfluent Vero E6 cells and incubated at 37 °C for 72 h. The CPE in each well was observed by microscope at 72 hpi, and the cell supernatants were collected in microfuge tubes (1.5 mL) and stored at −80 °C. Cannabinoid activity was compared with untreated cells not infected with the virus (cell control, 100% activity) and with untreated cells infected with the virus (virus only, 0% activity).

IC_{50} Determination by Tissue Culture Infectious Dose per mL Assay. Vero E6 cells were seeded in quadruplicate in a 96-well plate (2×10^4 cells/well) in DMEM supplemented with 10% FBS and antibiotics and incubated overnight at 37 °C in a 5% CO_2 incubator. The following day, the CPE assay medium from CBDA and its methyl ester conditions were serially diluted to 1:10 v/v in DMEM supplemented with 2% FBS and added to subconfluent Vero E6 cells, after decanting the existing supernatant. After 72 h, the $TCID_{50}$/mL value was calculated by using the Reed and Muench method,[28] and it was compared with the control represented by untreated cells infected with the virus (virus only) and cells infected and treated with vehicle control (DMSO). The results from three independent experiments were used to calculate the half-maximal inhibitory concentration (IC_{50}) by nonlinear regression curve using GraphPad Prism version 8.4.2.

qRT-PCR. The SARS-CoV-2 viral load was detected using the Allplex SARS-CoV-2 assay (Seegene, Seoul, Korea). RNA was extracted from supernatants using the STARMag Viral DNA/RNA 200 C kit (Seegene Technologies) with a Seegene STARlet extraction platform, and then the Allplex SARS-CoV-2 assay kit (Seegene Technologies) was used for detecting the E gene, RdRP/S gene, and N gene of SARS-CoV-2, according to the manufacturer's instructions. The absolute quantification (cp/μL) was calculated using the standard curve-based method that was generated by the determination of copy numbers from serial dilutions (10^7−10^0 copies) of the standard ssRNA (EURM-019) fragment of SARS-CoV-2.

Preparation of Cell Lysates. Vero E6 cells were treated for 72 h with CBDA (75.0 μM) and CBDA methyl ester (37.5 μM). A third group of cells was not treated with the compounds and was used as a control. Each treatment was performed in triplicate. After the treatments, cells were scraped and centrifuged to remove the supernatant. Then cell lysis was performed using cold MeOH (1 mL for 1×10^7 cells). Cells were then resuspended in cold MeOH, and cell lysis was promoted by sonication followed by freezing and thawing cycles. Finally, lysates were centrifuged at 15 000 rpm to remove cellular debris. In addition to lysates, culture media from the treatments were collected and analyzed by UHPLC-HRMS. Samples were stored at −80 °C until analysis.

UHPLC-HRMS Analysis of Cell Lysates. UHPLC-HRMS analysis of Vero E6 cell lysates and culture media was performed on a Thermo Scientific (MA, USA) UHPLC Ultimate 3000 equipped with a vacuum degasser, a binary pump, a thermostated autosampler, a thermostated column compartment, and a Q-Exactive Orbitrap mass spectrometer with a heated electrospray ionization (HESI) source. The analyses were carried out on an Ascentis Express C_{18} column (150 mm × 3.0 mm i.d., 2.7 μm, Supelco, Bellefonte, PA, USA), with a mobile phase composed of 0.1% HCOOH in both (A) H_2O and (B) ACN. The gradient elution was as follows: 0−13 min 60% B, 13−17 min from 60% to 80% B, 17−22 min from 80% to 90% B, which was kept for 8 min. The postrunning time was 10 min. The flow rate was 0.4 mL/min. The sample injection volume was 3 μL. The column temperature was 30 °C. MS acquisition was carried out with a HESI source operated in both the positive and negative ion modes. As to the MS detector, the source parameters were set as follows: sheath gas (N_2) 45, auxiliary gas (N_2) 25, auxiliary gas temperature 290 °C, electrospray voltage 3.8 kV (+) and 3.4 kV (−). The analyses were acquired in the full mass data-dependent (FM-dd-MS^2) mode at a resolving power of 17.500 full width at half-maximum (fwhm). The other mass analyzer parameters were set as follows: scan range m/z 100−2000, automatic grain control (AGC) target 1×10^6 (full MS) and 2×10^5 (FM-dd-MS^2) ions in the Orbitrap analyzer, ion injection time 200 ms (full MS) and 150 ms (FM-dd-MS^2), and isolation window for the filtration of the precursor ions m/z 1.0. The fragmentation of precursor ions was performed at 28 and 70 as normalized collision energies (NCE).

A standard mix of CBD, CBDA, and CBDA methyl ester was injected into the UHPLC system at a concentration of 1 ppm. Table 3 shows the MS and MS/MS parameters optimized for each compound.

Table 3. Retention Time and MS and MS/MS Data of the Target Compounds Monitored by UHPLC-HRMS[a]

compound	t_R (min)	$[M + H]^+$ (m/z)	$[M-H]^-$ (m/z)	MS/MS (m/z)
CBDA	14.7	—	357.2077	339.1966 (100), 107.0490 (83), 313.2176 (43)
CBD	17.4	315.2316	—	193.1221 (100), 123.0441 (73), 93.0702 (58)
CBDA methyl ester	23.2	—	371.2232	339.1965 (100), 170.0728 (31), 357.2073 (9)

[a]Compounds are shown in order of retention time.

Samples were diluted 1:10 v/v in the initial mobile phase before the analysis. The analyses were performed in duplicate for each sample.

***In Silico* Study of the Interaction with the SARS-CoV-2 Spike Protein.** The X-ray three-dimensional structure of SARS-CoV-2 spike receptor-binding domain complexed with its receptor ACE2 (PDBID: 6lzg) was obtained from the Protein Data Bank (PDB).[38]

The PDBFixer application, available in the OpenMM toolkit,[39] was used to add missing heavy atoms and missing hydrogen atoms, to build missing loops, and to convert nonstandard residues to their standard equivalents. The protein was prepared for docking using AutoDock Tools,[40] following the standard preparation protocol,[41] adding polar hydrogens, assigning Gasteiger−Marsili atomic charges,[42] and then merging nonpolar hydrogens.

The two-dimensional coordinates of CBDA and CBDA methyl ester were retrieved from PubChem[43] and then prepared using the LigPrep routine, by generating possible ionization and tautomeric states (pH ranging from 6.0 to 8.0), together with 200 conformations. Ligands were then converted to PDBQT format using OpenBabel.[44]

The protein was treated as rigid, and a blind docking approach was followed, by setting the grid box to encompass the whole protein structure (box center: x: −32.311, y: 25.835, z: 21.073) and sized to be 40 × 50 × 50 Å.

AutoDock Vina (v1.1.2) was used to perform the molecular docking simulations, setting the exhaustiveness to 24.[41]

Molecular graphics images were produced using the UCSF Chimera package from the Computer Graphics Laboratory, University of California, San Francisco.[45]

■ ASSOCIATED CONTENT

Supporting Information

The Supporting Information is available free of charge at https://pubs.acs.org/doi/10.1021/acs.jnatprod.3c00111.

^{1}H NMR spectra of the isolated and synthesized cannabinoids (Figures S1−S8). Cytotoxicity of cannabinoids (CC_{50}) toward Vero E6 Cells (Figure S9). Microscopic observation of the effect of CBDA and its

https://doi.org/10.1021/acs.jnatprod.3c00111
J. Nat. Prod. 2023, 86, 1698−1707

methyl ester on inhibition of CPE in Vero E6 cells infected with Italian strain SARS-CoV-2 PV10734 and VOCs (72 hpi) (Figure S10) (PDF)

AUTHOR INFORMATION

Corresponding Authors

Federica Pellati − *Department of Life Sciences, University of Modena and Reggio Emilia, 41125 Modena, Italy;* orcid.org/0000-0002-9822-6862; Phone: +39 059 2058565; Email: federica.pellati@unimore.it

Federica Pollastro − *Department of Pharmaceutical Sciences, University of Eastern Piedmont, 28100 Novara, Italy; PlantaChem srls, 28100 Novara, Italy;* orcid.org/0000-0002-0949-2799; Phone: +39 0321 375 844; Email: federica.pollastro@uniupo.it

Authors

Martina Tamburello − *Section of Microbiology, Department of Medical and Surgical Sciences (DIMEC), Alma Mater Studiorum University of Bologna, 40138 Bologna, Italy*

Stefano Salamone − *Department of Pharmaceutical Sciences, University of Eastern Piedmont, 28100 Novara, Italy; PlantaChem srls, 28100 Novara, Italy*

Lisa Anceschi − *Department of Life Sciences, University of Modena and Reggio Emilia, 41125 Modena, Italy; Clinical and Experimental Medicine PhD Program, University of Modena and Reggio, 41125 Modena, Italy*

Paolo Governa − *Department of Biotechnology, Chemistry and Pharmacy, University of Siena, 53100 Siena, Italy;* orcid.org/0000-0002-5976-780X

Virginia Brighenti − *Department of Life Sciences, University of Modena and Reggio Emilia, 41125 Modena, Italy*

Alice Morellini − *Section of Microbiology, Department of Medical and Surgical Sciences (DIMEC), Alma Mater Studiorum University of Bologna, 40138 Bologna, Italy;* orcid.org/0000-0003-4753-7916

Giada Rossini − *Microbiology Unit, IRCCS Azienda Ospedaliero-Universitaria di Bologna, 40138 Bologna, Italy*

Fabrizio Manetti − *Department of Biotechnology, Chemistry and Pharmacy, University of Siena, 53100 Siena, Italy;* orcid.org/0000-0002-9598-2339

Giorgio Gallinella − *Department of Pharmacy and Biotechnology, Alma Mater Studiorum University of Bologna, 40138 Bologna, Italy*

Complete contact information is available at: https://pubs.acs.org/10.1021/acs.jnatprod.3c00111

Notes

The authors declare no competing financial interest.

ACKNOWLEDGMENTS

Financial support for this work was provided by the PNNR Project One Health Basic and Translational Research Actions addressing Unmet Needs on Emerging Infectious Diseases, CUP B63C22001400007.

REFERENCES

(1) Li, H.; Liu, S. M.; Yu, X. H.; Tang, S. L.; Tang, C. *Int. J. Antimicrob. Agents* **2020**, *55*, 105951.

(2) Partridge, L. J.; Urwin, L.; Nicklin, M. J. H.; James, D. C.; Green, L. R.; Monk, P. N. *Cells* **2021**, *10*, 1419.

(3) Hoffmann, M.; Kleine-Weber, H.; Pöhlmann, S. *Mol. Cell* **2020**, *78*, 779−784.

(4) Zhou, Y. W.; Xie, Y.; Tang, L. S.; Pu, D.; Zhu, Y. J.; Liu, J. Y.; Ma, X. L. *Signal Transduct. Target. Ther.* **2021**, *6*, 317.

(5) Anand, U.; Jakhmola, S.; Indari, O.; Jha, H. C.; Chen, Z. S.; Tripathi, V.; Pérez de la Lastra, J. M. *Front. Immunol.* **2021**, *12*, 658519.

(6) Dong, L.; Hu, S.; Gao, J. *Drug Discovery Ther.* **2020**, *14*, 58−60.

(7) Singh, R.; Bhardwaj, V. K.; Sharma, J.; Kumar, D.; Purohit, R. *Comput. Biol. Med.* **2021**, *136*, 104631.

(8) Pellati, F.; Borgonetti, V.; Brighenti, V.; Biagi, M.; Benvenuti, S.; Corsi, L. *BioMed. Res. Int.* **2018**, 1691428.

(9) Hinz, B.; Ramer, R. *Br. J. Cancer* **2022**, *127*, 1−13.

(10) Hill, K. P. *Cannabis Cannabinoid Res.* **2020**, *5*, 118−120.

(11) Mabou Tagne, A.; Pacchetti, B.; Sodergren, M.; Cosentino, M.; Marino, F. *Cannabis Cannabinoid Res.* **2020**, *5*, 121−131.

(12) D'Elia, R. V.; Harrison, K.; Oyston, P. C.; Lukaszewski, R. A.; Clark, G. C. *Clin. Vaccine Immunol.* **2013**, *20*, 319−327.

(13) Mahmud, M. S.; Hossain, M. S.; Ahmed, A. T. M. F.; Islam, M. Z.; Sarker, M. E.; Islam, M. R. *Molecules* **2021**, *26*, 7216.

(14) Onaivi, E. S.; Sharma, V. *Future Sci. OA* **2020**, *6*, FSO625.

(15) Khattab, A. R.; Teleb, M. *Future Virol.* **2022**, *17*, 367−386.

(16) Altyar, A. E.; Youssef, F. S.; Kurdi, M. M.; Bifari, R. J.; Ashour, M. L. *Molecules* **2022**, *27*, 2797.

(17) Raj, V.; Park, J. G.; Cho, K. H.; Choi, P.; Kim, T.; Ham, J.; Lee, J. *Int. J. Biol. Macromol.* **2021**, *168*, 474−485.

(18) Anil, S. M.; Shalev, N.; Vinayaka, A. C.; Stalin Nadarajan, S.; Namdar, D.; Belausov, E.; Shoval, I.; Mani, K. A.; Mechrez, G.; Koltai, H. *Sci. Rep.* **2021**, *11*, 1462.

(19) Nguyen, L. C.; Yang, D.; Nicolaescu, V.; Best, T. J.; Gula, H.; Saxena, D.; Gabbard, J. D.; Chen, S. N.; Ohtsuki, T.; Friesen, J. B.; Drayman, N.; Mohamed, A.; Dann, C.; Silva, D.; Robinson-Mailman, L.; Valdespino, A.; Stock, L.; Suárez, E.; Jones, K. A.; Azizi, S. A.; Demarco, J. K.; Severson, W. E.; Anderson, C. D.; Millis, J. M.; Dickinson, B. C.; Tay, S.; Oakes, S. A.; Pauli, G. F.; Palmer, K. E. *Sci. Adv.* **2022**, *8*, No. eabi6110.

(20) Wang, B.; Kovalchuk, A.; Li, D.; Rodriguez-Juarez, R.; Ilnytskyy, Y.; Kovalchuk, I.; Kovalchuk, O. *Aging* **2020**, *12*, 22425−22444.

(21) van Breemen, R. B.; Muchiri, R. N.; Bates, T. A.; Weinstein, J. B.; Leier, H. C.; Farley, S.; Tafesse, F. G. *J. Nat. Prod.* **2022**, *85*, 176−184.

(22) Ben-Cnaan, E.; Permyakova, A.; Azar, S.; Hirsch, S.; Baraghithy, S.; Hinden, L.; Tam, J. *Int. J. Mol. Sci.* **2022**, *23*, 5610.

(23) Hanuš, L. O.; Meyer, S. M.; Muñoz, E.; Taglialatela-Scafati, O.; Appendino, G. *Nat. Prod. Rep.* **2016**, *33*, 1357−1392.

(24) Yan, K.; Rawle, D. J.; Le, T. T.; Suhrbier, A. *Virol. J.* **2021**, *18*, 123.

(25) Zhu, N.; Wang, W.; Liu, Z.; Liang, C.; Wang, W.; Ye, F.; Huang, B.; Zhao, L.; Wang, H.; Zhou, W.; Deng, Y.; Mao, L.; Su, C.; Qiang, G.; Jiang, T.; Zhao, J.; Wu, G.; Song, J.; Tan, W. *Nat. Commun.* **2020**, *11*, 3910.

(26) Severson, W. E.; Shindo, N.; Sosa, M.; Fletcher, I. T.; White, E. L.; Ananthan, S.; Jonsson, C. B. *SLAS Discovery* **2007**, *12*, 33−40.

(27) Familletti, P. C.; Rubinstein, S.; Pestka, S. A. *Meth. Enzymol.* **1981**, *78*, 387−394.

(28) Lei, C.; Yang, J.; Hu, J.; Sun, X. *Virol. Sin.* **2021**, *36*, 141−144.

(29) Stelzer-Braid, S.; Walker, G. J.; Aggarwal, A.; Isaacs, S. R.; Yeang, M.; Naing, Z.; Ospina Stella, A.; Turville, S. G.; Rawlinson, W. D. *Pathology* **2020**, *52*, 760−763.

(30) Amanat, F.; White, K. M.; Miorin, L.; Strohmeier, S.; McMahon, M.; Meade, P.; Liu, W.; Albrecht, R. A.; Simon, V.; Martinez-Sobrido, L.; Moran, T.; García-Sastre, A.; Krammer, F. *Curr. Protoc. Microbiol.* **2020**, *58*, No. e108.

(31) Brandolini, M.; Taddei, F.; Marino, M. M.; Grumiro, L.; Scalcione, A.; Turba, M. E.; Gentilini, F.; Fantini, M.; Zannoli, S.; Dirani, G.; Sambri, V. *Viruses* **2021**, *13*, 1022.

(32) Mechoulam, R.; Gaoni, Y. H., IV. *Tetrahedron* **1965**, *21*, 1223−1229.

(33) Choi, Y. H.; Hazekamp, A.; Peltenburg-Looman, A. M. G.; Frédérich, M.; Erkelens, C.; Lefeber, A. V. M.; Verpoorte, R. *Phytochem. Anal.* **2004**, *15*, 345−354.
(34) Claussen, U.; Von Spulak, F.; Korte, F. *Tetrahedron* **1966**, *22*, 1477−1479.
(35) Shoyama, Y.; Hirano, H.; Makino, H.; Umekita, N.; Nishioka, I. *Chem. Pharm. Bull.* **1977**, *25*, 2306−2311.
(36) Alteri, C.; Cento, V.; Piralla, A.; Costabile, V.; Tallarita, M.; Colagrossi, L.; Renica, S.; Giardina, F.; Novazzi, F.; Gaiarsa, S.; Matarazzo, E.; Antonello, M.; Vismara, C.; Fumagalli, R.; Epis, O. M.; Puoti, M.; Perno, C. F.; Baldanti, F. *Nat. Commun.* **2021**, *12*, 434.
(37) Case, J. B.; Bailey, A. L.; Kim, A. S.; Chen, R. E.; Diamond, M. S. *Virology* **2020**, *548*, 39−48.
(38) Berman, H. M.; Westbrook, J.; Feng, Z.; Gilliland, G.; Bhat, T. N.; Weissig, H.; Shindyalov, I. N.; Bourne, P. E. *Nucleic Acids Res.* **2000**, *28*, 235−242.
(39) Eastman, P.; Swails, J.; Chodera, J. D.; McGibbon, R. T.; Zhao, Y.; Beauchamp, K. A.; Wang, L.-P.; Simmonett, A. C.; Harrigan, M. P.; Stern, C. D.; Wiewiora, R. P.; Brooks, B. R.; Pande, V. S. *PLOS Comput. Biol.* **2017**, *13*, No. e1005659.
(40) Morris, G. M.; Huey, R.; Lindstrom, W.; Sanner, M. F.; Belew, R. K.; Goodsell, D. S.; Olson, A. J. *J. Comput. Chem.* **2009**, *30*, 2785−2791.
(41) Forli, S.; Huey, R.; Pique, M. E.; Sanner, M. F.; Goodsell, D. S.; Olson, A. J. *Nat. Protoc.* **2016**, *11*, 905−919.
(42) Gasteiger, J.; Marsili, M. *Tetrahedron* **1980**, *36*, 3219−3228.
(43) Kim, S.; Chen, J.; Cheng, T.; Gindulyte, A.; He, J.; He, S.; Li, Q.; Shoemaker, B. A.; Thiessen, P. A.; Yu, B.; Zaslavsky, L.; Zhang, J.; Zhang, J.; Bolton, E. E. *Nucleic Acid Res.* **2023**, *51*, D1373−D1380.
(44) O'Boyle, N. M.; Banck, M.; James, C. A.; Morley, C.; Vandermeersch, T.; Hutchison, G. R. *J. Cheminformatics* **2011**, *3*, 33.
(45) Pettersen, E. F.; Goddard, T. D.; Huang, C. C.; Couch, G. S.; Greenblatt, D. M.; Meng, E. C.; Ferrin, T. E. *J. Comput. Chem.* **2004**, *25*, 1605−1612.

https://doi.org/10.1021/acs.jnatprod.3c00111
J. Nat. Prod. 2023, 86, 1698−1707